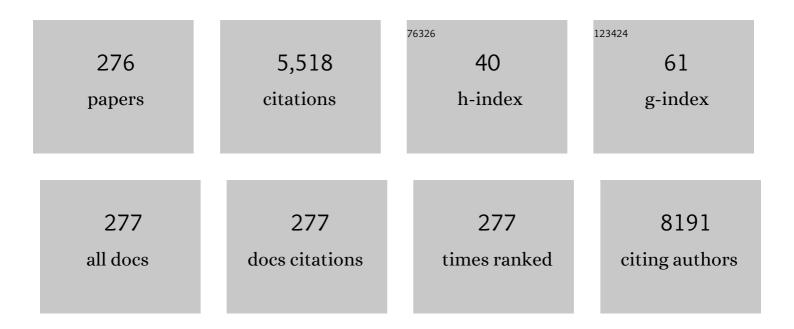
List of Publications by Year in descending order

Source: https://exaly.com/author-pdf/8533200/publications.pdf Version: 2024-02-01



Ιλε Ηνιίνι Κιμ

#	Article	IF	CITATIONS
1	Magnetic properties of epitaxially grown semiconducting Zn1â <sup>~</sup> 'xCoxO thin films by pulsed laser deposition. Journal of Applied Physics, 2002, 92, 6066-6071.	2.5	323
2	Mechanism Study of ZnO Nanorod-Bundle Sensors for H <sub>2</sub> S Gas Sensing. Journal of Physical Chemistry C, 2011, 115, 7218-7224.	3.1	261
3	CuO/ZnO Heterostructured Nanorods: Photochemical Synthesis and the Mechanism of H <sub>2</sub> S Gas Sensing. Journal of Physical Chemistry C, 2012, 116, 15682-15691.	3.1	188
4	Highly Sensitive and Multifunctional Tactile Sensor Using Free-standing ZnO/PVDF Thin Film with Graphene Electrodes for Pressure and Temperature Monitoring. Scientific Reports, 2015, 5, 7887.	3.3	160
5	Exploring Rapid Photocatalytic Degradation of Organic Pollutants with Porous CuO Nanosheets: Synthesis, Dye Removal, and Kinetic Studies at Room Temperature. ACS Omega, 2021, 6, 2601-2612.	3.5	117
6	Duplex Bioelectronic Tongue for Sensing Umami and Sweet Tastes Based on Human Taste Receptor Nanovesicles. ACS Nano, 2016, 10, 7287-7296.	14.6	78
7	Double-layer CVD graphene as stretchable transparent electrodes. Nanoscale, 2014, 6, 6057-6064.	5.6	77
8	Extraction of diode parameters of silicon solar cells under high illumination conditions. Energy Conversion and Management, 2013, 76, 421-429.	9.2	74
9	Intensity dependency of photovoltaic cell parameters under high illumination conditions: An analysis. Applied Energy, 2014, 133, 356-362.	10.1	74
10	Control of leucine-dependent mTORC1 pathway through chemical intervention of leucyl-tRNA synthetase and RagD interaction. Nature Communications, 2017, 8, 732.	12.8	71
11	Effects of metformin on colorectal cancer stem cells depend on alterations in glutamine metabolism. Scientific Reports, 2018, 8, 409.	3.3	70
12	Recent progress in terahertz difference-frequency quantum cascade laser sources. Nanophotonics, 2018, 7, 1795-1817.	6.0	67
13	Electrochemically deposited Fe2O3 nanorods on carbon nanofibers for free-standing anodes of lithium-ion batteries. Carbon, 2015, 94, 9-17.	10.3	66
14	Hierarchical ZnO Nanorods on Si Micropillar Arrays for Performance Enhancement of Piezoelectric Nanogenerators. ACS Applied Materials & Interfaces, 2015, 7, 5768-5774.	8.0	65
15	Optical and magnetic properties of laser-deposited Co-doped ZnO thin films. Solid State Communications, 2004, 131, 677-680.	1.9	64
16	Ultraconformal Contact Transfer of Monolayer Graphene on Metal to Various Substrates. Advanced Materials, 2014, 26, 6394-6400.	21.0	63
17	Enhanced cycle stability of polypyrrole-derived nitrogen-doped carbon-coated tin oxide hollow nanofibers for lithium battery anodes. Carbon, 2017, 111, 28-37.	10.3	63
18	Low Temperature Atomic Layer Deposition of Ruthenium Thin Films Using Isopropylmethylbenzene-Cyclohexadiene-Ruthenium and O[sub 2]. Electrochemical and Solid-State Letters, 2009, 12, D85.	2.2	62

#	Article	IF	CITATIONS
19	Mechanical and Environmental Stability of Polymer Thin-Film-Coated Graphene. ACS Nano, 2012, 6, 2096-2103.	14.6	61
20	Wide range temperature dependence of analytical photovoltaic cell parameters for silicon solar cells under high illumination conditions. Applied Energy, 2016, 183, 715-724.	10.1	61
21	Enhanced electrochemical performance of template-free carbon-coated iron(II, III) oxide hollow nanofibers as anode material for lithium-ion batteries. Journal of Power Sources, 2015, 284, 392-399.	7.8	57
22	Physical Characterization and In Vitro Biological Impact of Highly Aggregated Antibodies Separated into Size-Enriched Populations by Fluorescence-Activated Cell Sorting. Journal of Pharmaceutical Sciences, 2015, 104, 1575-1591.	3.3	57
23	Nitrogen and sulfur co-doped metal monochalcogen encapsulated honeycomb like carbon nanostructure as a high performance lithium-ion battery anode material. Carbon, 2017, 115, 249-260.	10.3	57
24	N-functionalized graphene quantum dots: Charge transporting layer for high-rate and durable Li4Ti5O12-based Li-ion battery. Chemical Engineering Journal, 2019, 369, 1024-1033.	12.7	55
25	Highly stable enzyme precipitate coatings and their electrochemical applications. Biosensors and Bioelectronics, 2011, 26, 1980-1986.	10.1	54
26	Synthesis of biolubricants using sulfated zirconia catalysts. Applied Catalysis A: General, 2013, 455, 164-171.	4.3	54
27	Multiplexed femtomolar detection of Alzheimer's disease biomarkers in biofluids using a reduced graphene oxide field-effect transistor. Biosensors and Bioelectronics, 2020, 167, 112505.	10.1	54
28	Improved electrochemical performance of boron-doped SiO negative electrode materials in lithium-ion batteries. Journal of Power Sources, 2015, 299, 25-31.	7.8	52
29	The origin of room temperature ferromagnetism in cobalt-doped zinc oxide thin films fabricated by PLD. Journal of the European Ceramic Society, 2004, 24, 1847-1851.	5.7	51
30	Stacked Bilayer Graphene and Redox-Active Interlayer for Transparent and Flexible High-Performance Supercapacitors. Chemistry of Materials, 2015, 27, 3621-3627.	6.7	50
31	Tunable Electrical and Optical Properties in Composition Controlled Hf:ZnO Thin Films Grown by Atomic Layer Deposition. Journal of the Electrochemical Society, 2012, 159, H384-H387.	2.9	48
32	Visible emission from Ce-doped ZnO nanorods grown by hydrothermal method without a post thermal annealing process. Nanoscale Research Letters, 2012, 7, 43.	5.7	48
33	Facile synthesis of Ag-coated silicon nanowires as anode materials for high-performance rechargeable lithium battery. Journal of Alloys and Compounds, 2016, 660, 387-391.	5.5	47
34	Effects of preoperative ultrasound-guided transversus abdominis plane block on pain after laparoscopic surgery for colorectal cancer: a double-blind randomized controlled trial. Surgical Endoscopy and Other Interventional Techniques, 2017, 31, 127-134.	2.4	47
35	Nanoscale enzyme reactors in mesoporous carbon for improved performance and lifetime of biosensors and biofuel cells. Biosensors and Bioelectronics, 2010, 26, 655-660.	10.1	45
36	Preparation of hybrid silicon wire and planar solar cells having ZnO antireflection coating by all-solution processes. Solar Energy Materials and Solar Cells, 2012, 96, 251-256.	6.2	44

#	Article	IF	CITATIONS
37	Performance enhancement of triboelectric nanogenerators based on polyvinylidene fluoride/graphene quantum dot composite nanofibers. Journal of Alloys and Compounds, 2019, 797, 945-951.	5.5	44
38	Conformal Coating of Conductive ZnO:Al Films as Transparent Electrodes on High Aspect Ratio Si Microrods. Electrochemical and Solid-State Letters, 2010, 13, K12.	2.2	43
39	Characterization of the Physical Stability of a Lyophilized IgG1 mAb after Accelerated Shipping-Like Stress. Journal of Pharmaceutical Sciences, 2015, 104, 495-507.	3.3	43
40	Improved data visualization techniques for analyzing macromolecule structural changes. Protein Science, 2012, 21, 1540-1553.	7.6	42
41	Effect of Ionic Strength and pH on the Physical and Chemical Stability of a Monoclonal Antibody Antigen-Binding Fragment. Journal of Pharmaceutical Sciences, 2013, 102, 2520-2537.	3.3	40
42	Effective passivation of silicon surface by AZO films: Application in bifacial solar cells. Solar Energy, 2013, 97, 474-483.	6.1	40
43	Low-temperature annealed PbS quantum dot films for scalable and flexible ambipolar thin-film-transistors and circuits. Journal of Materials Chemistry C, 2014, 2, 10305-10311.	5.5	40
44	Miniature Cone Tip Resistance on Sand in a Centrifuge. Journal of Geotechnical and Geoenvironmental Engineering - ASCE, 2016, 142, .	3.0	40
45	Effects of a dopant on the electrochemical properties of Li4Ti5O12 as a lithium-ion battery anode material. Journal of Power Sources, 2013, 244, 527-531.	7.8	38
46	Enhanced charge transport properties of Ag and Al co-doped ZnO nanostructures via solution process. Journal of Alloys and Compounds, 2016, 682, 232-237.	5.5	38
47	Radar Chart Array Analysis to Visualize Effects of Formulation Variables on IgG1 Particle Formation as Measured by Multiple Analytical Techniques. Journal of Pharmaceutical Sciences, 2013, 102, 4256-4267.	3.3	37
48	Monatomic Chemical-Vapor-Deposited Graphene Membranes Bridge a Half-Millimeter-Scale Gap. ACS Nano, 2014, 8, 2336-2344.	14.6	37
49	Precipitated and chemically-crosslinked laccase over polyaniline nanofiber for high performance phenol sensing. Chemosphere, 2016, 143, 142-147.	8.2	37
50	Highly selective FET-type glucose sensor based on shape-controlled palladium nanoflower-decorated graphene. Sensors and Actuators B: Chemical, 2018, 264, 216-223.	7.8	37
51	N-Functionalized Graphene Quantum Dots with Ultrahigh Quantum Yield and Large Stokes Shift: Efficient Downconverters for CIGS Solar Cells. ACS Photonics, 2018, 5, 4637-4643.	6.6	37
52	Influence of oxygen vacancies on surface charge potential and transportation properties of Al-doped ZnO nanostructures produced via atomic layer deposition. Journal of Alloys and Compounds, 2017, 709, 819-828.	5.5	35
53	Characterization of hafnium silicate thin films grown by MOCVD using a new combination of precursors. Journal of Crystal Growth, 2004, 263, 442-446.	1.5	34
54	Spectral purity and tunability of terahertz quantum cascade laser sources based on intracavity difference-frequency generation. Science Advances, 2017, 3, e1603317.	10.3	33

#	Article	IF	CITATIONS
55	Technological advances in electrochemical biosensors for the detection of disease biomarkers. Biomedical Engineering Letters, 2021, 11, 309-334.	4.1	33
56	Influence of Ag doping on structural, optical, and photoluminescence properties of nanostructured AZO films by sol–gel technique. Journal of Alloys and Compounds, 2014, 584, 190-194.	5.5	32
57	Spectroscopic Study of Terahertz Generation in Mid-Infrared Quantum Cascade Lasers. Scientific Reports, 2016, 6, 21169.	3.3	32
58	Fabrication of Uniform Wrinkled Silica Nanoparticles and Their Application to Abrasives in Chemical Mechanical Planarization. ACS Applied Materials & amp; Interfaces, 2018, 10, 11843-11851.	8.0	32
59	High-Throughput Biophysical Analysis and Data Visualization of Conformational Stability of an IgG1 Monoclonal Antibody After Deglycosylation. Journal of Pharmaceutical Sciences, 2013, 102, 3942-3956.	3.3	31
60	Physical Stability Comparisons of IgG1-Fc Variants: Effects of N-Glycosylation Site Occupancy and Asp/Gln Residues at Site Asn 297. Journal of Pharmaceutical Sciences, 2014, 103, 1613-1627.	3.3	31
61	A low temperature process for phosphorous doped ZnO nanorods via a combination of hydrothermal and spin-on dopant methods. Nanoscale, 2014, 6, 2046-2051.	5.6	31
62	Transparent conductive ZnO:Al films grown by atomic layer deposition for Si-wire-based solar cells. Current Applied Physics, 2012, 12, 273-279.	2.4	30
63	A Novel Algorithm for Zero Block Detection in High Efficiency Video Coding. IEEE Journal on Selected Topics in Signal Processing, 2013, 7, 1124-1134.	10.8	30
64	Enzyme precipitate coating of pyranose oxidase on carbon nanotubes and their electrochemical applications. Biosensors and Bioelectronics, 2017, 87, 365-372.	10.1	29
65	Enhancement of the ionic conductivity of a composite polymer electrolyte <i>via</i> surface functionalization of SSZ-13 zeolite for all-solid-state Li-metal batteries. Journal of Materials Chemistry A, 2021, 9, 4126-4137.	10.3	29
66	Analysis of PV cell parameters of solution processed Cu-doped nickel oxide hole transporting layer-based organic-inorganic perovskite solar cells. Solar Energy, 2020, 209, 226-234.	6.1	28
67	Characterization of Zirconium Silicate Gate Dielectrics Deposited on Si(100) Using Zr(NEt[sub 2])[sub 4] and Si(O[sup n]Bu)[sub 4]. Electrochemical and Solid-State Letters, 2004, 7, F35.	2.2	27
68	Catalytic activity of carbon-sphere/Co3O4/RuO2 nanocomposite for Li-air batteries. Journal of Electroceramics, 2013, 31, 224-230.	2.0	27
69	Characterization and Protective Efficacy of Type III Secretion Proteins as a Broadly Protective Subunit Vaccine against Salmonella enterica Serotypes. Infection and Immunity, 2018, 86, .	2.2	27
70	Enhanced performance of silicon solar cells by application of low-cost sol–gel-derived Al-rich ZnO film. Solar Energy, 2014, 101, 265-271.	6.1	26
71	Characterization of optical absorption and photovoltaic properties of silicon wire solar cells with different aspect ratio. Current Applied Physics, 2011, 11, S30-S33.	2.4	25
72	Enhanced electrochemical sensitivity of enzyme precipitate coating (EPC)-based glucose oxidase biosensors with increased free CNT loadings. Bioelectrochemistry, 2015, 101, 114-119.	4.6	25

#	Article	IF	CITATIONS
73	One-step and controllable bipolar doping of reduced graphene oxide using TMAH as reducing agent and doping source for field effect transistors. Carbon, 2016, 100, 608-616.	10.3	25
74	Terahertz difference-frequency quantum cascade laser sources on silicon. Optica, 2017, 4, 38.	9.3	25
75	An empirical phase diagram approach to investigate conformational stability of "secondâ€generation― functional mutants of acidic fibroblast growth factorâ€1. Protein Science, 2012, 21, 418-432.	7.6	24
76	High-Purity Ultraviolet Electroluminescence from <i>n</i> -ZnO Nanowires/ <i>p</i> <sup>+</sup> -Si Heterostructure LEDs with <i>i</i> -MgO Film as Carrier Control Layer. Journal of the Electrochemical Society, 2011, 159, H102-H106.	2.9	23
77	A facile, coverage controlled deposition of Au nanoparticles on ZnO nanorods by sonochemical reaction for enhancement of photocatalytic activity. Journal of Nanoparticle Research, 2012, 14, 1.	1.9	23
78	Ultimate Control of Rate-Dependent Adhesion for Reversible Transfer Process via a Thin Elastomeric Layer. ACS Applied Materials & Interfaces, 2017, 9, 12886-12892.	8.0	23
79	Growth of ZnO nanorod arrays by hydrothermal method using homoâ€seed layers annealed at various temperatures. Surface and Interface Analysis, 2010, 42, 978-982.	1.8	22
80	Fabrication and characterization of silicon wire solar cells having ZnO nanorod antireflection coating on Al-doped ZnO seed layer. Nanoscale Research Letters, 2012, 7, 29.	5.7	22
81	Comparative experimental and simulative investigations of radial p–n junction Si microwire array solar cells. Solar Energy Materials and Solar Cells, 2012, 103, 93-97.	6.2	22
82	Multiwavelength Raman characterization of silicon stress near through-silicon vias and its inline monitoring applications. Journal of Micro/ Nanolithography, MEMS, and MOEMS, 2014, 13, 011205.	0.9	22
83	Conductive framework supported high rate performance of SnO2 hollow nanofibers for lithium battery anodes. Electrochimica Acta, 2015, 161, 1-9.	5.2	22
84	Local Dynamics and Their Alteration by Excipients Modulate the Global Conformational Stability of an lgG1 Monoclonal Antibody. Journal of Pharmaceutical Sciences, 2012, 101, 4444-4457.	3.3	21
85	Preformulation Study of Highly Purified Inactivated Polio Vaccine, Serotype 3. Journal of Pharmaceutical Sciences, 2014, 103, 140-151.	3.3	21
86	Impact of Detergent on Biophysical Properties and Immune Response of the IpaDB Fusion Protein, a Candidate Subunit Vaccine against Shigella Species. Infection and Immunity, 2015, 83, 292-299.	2.2	21
87	Performance Degradation Analysis of c-Si PV Modules Mounted on a Concrete Slab under Hot-Humid Conditions Using Electroluminescence Scanning Technique for Potential Utilization in Future Solar Roadways. Materials, 2019, 12, 4047.	2.9	21
88	Enhanced charge-transportation properties of low-temperature processed Al-doped ZnO and its impact on PV cell parameters of organic-inorganic perovskite solar cells. Solid-State Electronics, 2020, 164, 107714.	1.4	21
89	Immobilization of glucose oxidase on graphene oxide for highly sensitive biosensors. Biotechnology and Bioprocess Engineering, 2016, 21, 573-579.	2.6	20
90	Influence of nickel oxide nanolayer and doping in organic light-emitting devices. Journal of Industrial and Engineering Chemistry, 2009, 15, 716-718.	5.8	19

#	Article	IF	CITATIONS
91	One-step etching, doping, and adhesion-control process for graphene electrodes. Carbon, 2015, 82, 168-175.	10.3	19
92	Fabrication of precisely controlled silicon wire and cone arrays by electrochemical etching. Materials Letters, 2009, 63, 2567-2569.	2.6	18
93	Optimization of metal-assisted chemical etching process in fabrication of p-type silicon wire arrays. Current Applied Physics, 2011, 11, S25-S29.	2.4	18
94	Enhanced electrochemical performance of carbon-coated TiO2 nanobarbed fibers as anode material for lithium-ion batteries. Electrochemistry Communications, 2015, 60, 204-207.	4.7	18
95	Quantum cascade lasers transfer-printed on silicon-on-sapphire. Applied Physics Letters, 2017, 111, .	3.3	18
96	Emission-wavelength-dependent photoluminescence decay lifetime of N-functionalized graphene quantum dot downconverters: Impact on conversion efficiency of Cu(In, Ga)Se2 solar cells. Scientific Reports, 2019, 9, 10803.	3.3	18
97	LOW-TEMPERATURE SYNTHESIZED <font>ZnO</font> NANONEEDLES: XPS AND PL ANALYSIS. Surface Review and Letters, 2007, 14, 1061-1065.	1.1	17
98	Widely tunable terahertz source based on intra-cavity frequency mixing in quantum cascade laser arrays. Applied Physics Letters, 2015, 106, .	3.3	17
99	Three-dimensional Macropore Arrays in \$p\$-type Silicon Fabricated by Electrochemical Etching. Journal of the Korean Physical Society, 2009, 55, 5-9.	0.7	17
100	Enhanced compatibility of a polymer-based electrolyte with Li-metal for stable and dendrite-free all-solid-state Li-metal batteries. Journal of Materials Chemistry A, 2021, 9, 27304-27319.	10.3	17
101	Atomic Layer Chemical Vapor Deposition and Electrical Characterization of Hafnium Silicate Films. Journal of the Electrochemical Society, 2005, 152, F45.	2.9	16
102	Analysis of photovoltaic cell parameters of non-vacuum solution processed Cu(In, Ga)Se 2 thin film based solar cells. Solar Energy, 2014, 108, 189-198.	6.1	16
103	Reliability Study of c-Si PV Module Mounted on a Concrete Slab by Thermal Cycling Using Electroluminescence Scanning: Application in Future Solar Roadways. Materials, 2020, 13, 470.	2.9	16
104	Fluorescent N-Doped Graphene Quantum Dots Embedded in Transparent Polymer Films for Photon-Downconversion Applications. ACS Applied Nano Materials, 2020, 3, 2322-2335.	5.0	16
105	The Design of Photosensitive Polyimide Materials for Buffer Coating Processes. Journal of Photopolymer Science and Technology = [Fotoporima Konwakai Shi], 2009, 22, 403-405.	0.3	15
106	Dual Heteroatomâ€Doped Carbon Nanofoamâ€Wrapped Iron Monosulfide Nanoparticles: An Efficient Cathode Catalyst for Li–O <sub>2</sub> Batteries. ChemSusChem, 2017, 10, 1554-1562.	6.8	15
107	Physical and electrical characterizations of ultrathin Si-rich Hf-silicate film and Hf-silicate/SiO2 bilayer deposited by atomic layer chemical vapor deposition. Journal of Applied Physics, 2006, 100, 044106.	2.5	14
108	Role of HbA1c in the Screening of Diabetes Mellitus in a Korean Rural Community. Diabetes and Metabolism Journal, 2012, 36, 37.	4.7	14

#	Article	IF	CITATIONS
109	Dewetted gold nanoparticles on ZnO nanorods for three-dimensionally distributed plasmonic hot spots. Scripta Materialia, 2013, 69, 654-657.	5.2	14
110	Influence of Al content on surface passivation properties of Al rich ZnO films for solar cell application. Solar Energy, 2014, 110, 595-602.	6.1	14
111	Programmable multimedia platform based on reconfigurable processor for 8K UHD TV. IEEE Transactions on Consumer Electronics, 2015, 61, 516-523.	3.6	13
112	Effect of loading pattern on longitudinal bowing in flexible roll forming. Journal of Mechanical Science and Technology, 2016, 30, 5633-5639.	1.5	13
113	Development of Three-Dimensional Nickel–Cobalt Oxide Nanoflowers for Superior Photocatalytic Degradation of Food Colorant Dyes: Catalyst Properties and Reaction Kinetic Study. Langmuir, 2021, 37, 12929-12939.	3.5	13
114	Coefficient of thermal expansion measurements for freestanding nanocrystalline ultra-thin gold films. International Journal of Precision Engineering and Manufacturing, 2014, 15, 105-110.	2.2	12
115	Paraboloid Structured Silicon Surface for Enhanced Light Absorption: Experimental and Simulative Investigations. Nanoscale Research Letters, 2015, 10, 376.	5.7	12
116	Novel approach for fabrication of buried contact silicon nanowire solar cells with improved performance. Solar Energy, 2016, 137, 122-128.	6.1	12
117	Size-dependent hardness of five-fold twin structured Ag nanowires. Physical Chemistry Chemical Physics, 2017, 19, 1311-1319.	2.8	12
118	Structural color and near-infrared tunability of ruthenium-coated anodic aluminum oxide by atomic layer deposition. Scripta Materialia, 2020, 187, 125-129.	5.2	12
119	Thermal decomposition pathway and desorption study of isopropanol andtert-butanol on Si(100). Journal of Vacuum Science and Technology A: Vacuum, Surfaces and Films, 2002, 20, 1582-1586.	2.1	11
120	ZnO Wurtzite Single Crystals Prepared by Nanorod-Assisted Epitaxial Lateral Overgrowth. Crystal Growth and Design, 2010, 10, 321-326.	3.0	11
121	Influence of the crystallographic orientation of silicon nanowires in a carbon matrix on electrochemical performance as negative electrode materials for lithium-ion batteries. Journal of Power Sources, 2013, 244, 515-520.	7.8	11
122	Photo-assisted molecular engineering in solution-processed organic thin-film transistors with a blended semiconductor for high mobility anisotropy. Applied Physics Letters, 2013, 102, 013306.	3.3	11
123	Optimal design of organic–inorganic hybrid tandem solar cell based on a‧i:H and organic photovoltaics for high efficiency. Micro and Nano Letters, 2014, 9, 881-883.	1.3	11
124	Correlation between reflectance and photoluminescent properties of al-rich ZnO nano-structures. Metals and Materials International, 2015, 21, 561-568.	3.4	11
125	Materialization of strained CVD-graphene using thermal mismatch. Nano Research, 2015, 8, 2082-2091.	10.4	11
126	High Performance Flexible Actuator of Urchinâ€Like ZnO Nanostructure/Polyvinylenefluoride Hybrid Thin Film with Graphene Electrodes for Acoustic Generator and Analyzer, Small, 2016, 12, 2567-2574	10.0	11

#	Article	IF	CITATIONS
127	Biosimilarity Assessments of Model IgG1-Fc Glycoforms Using a Machine Learning Approach. Journal of Pharmaceutical Sciences, 2016, 105, 602-612.	3.3	11
128	Investigation of the surface passivation mechanism through an Ag-doped Al-rich film using a solution process. Nanoscale, 2016, 8, 1007-1014.	5.6	11
129	Reduction of permanent image sticking in ACPDPs using RFâ€plasma pretreatment on MgO surface. Journal of the Society for Information Display, 2010, 18, 606-613.	2.1	10
130	Combinational Approach of Electrochemical Etching and Metal-Assisted Chemical Etching for p-Type Silicon Wire Formation. Electrochemical and Solid-State Letters, 2011, 14, D5.	2.2	10
131	Electrochemical Activity Studies of Glucose Oxidase (GOx)-Based and Pyranose Oxidase (POx)-Based Electrodes in Mesoporous Carbon: Toward Biosensor and Biofuel Cell Applications. Electroanalysis, 2014, 26, 2075-2079.	2.9	10
132	A study on the development of post processor for five-axis machining using angle head spindle. International Journal of Precision Engineering and Manufacturing, 2015, 16, 2683-2689.	2.2	10
133	Work function tuning and fluorescence enhancement of hydrogen annealed Ag-doped Al-rich zinc oxide nanostructures using a sol–gel process. Journal of Alloys and Compounds, 2015, 647, 566-572.	5.5	10
134	Effect of Si nanostructures on PEDOT:PSS Si hybrid solar cells. Thin Solid Films, 2016, 616, 335-338.	1.8	10
135	Fabrication of Shapeâ€Controlled Palladium Nanoparticleâ€Decorated Electrospun Polypyrrole/Polyacrylonitrile Nanofibers for Hydrogen Peroxide Coalescing Detection. Advanced Materials Interfaces, 2017, 4, 1700573.	3.7	10
136	Double-metal waveguide terahertz difference-frequency generation quantum cascade lasers with surface grating outcouplers. Applied Physics Letters, 2018, 113, 161102.	3.3	10
137	UV-Curable Polymer–QD Flexible Films as the Downconversion Layer for Improved Performance of Cu(In,Ga)Se <sub>2</sub> Solar Cells. Energy & Fuels, 2020, 34, 14581-14590.	5.1	10
138	Interfacial Properties of Hf-silicateâ^•Si and Hf-silicateâ^•Al[sub 2]0[sub 3]â^•Si Deposited by Atomic Layer Chemical Vapor Deposition. Journal of the Electrochemical Society, 2005, 152, F153.	2.9	9
139	Biophysical Characterization of the Type III Secretion Tip Proteins and the Tip Proteins Attached to Bacterium-Like Particles. Journal of Pharmaceutical Sciences, 2015, 104, 424-432.	3.3	9
140	Biophysical Characterization of the Type III Secretion System Translocator Proteins and the Translocator Proteins Attached to Bacterium-Like Particles. Journal of Pharmaceutical Sciences, 2015, 104, 4065-4073.	3.3	9
141	Electron beam modification of anode materials for high-rate lithium ion batteries. Journal of Power Sources, 2015, 296, 109-116.	7.8	9
142	Ionic Conductivity of Ruddlesdenâ€Popper Layered Perovskites (Li <sub>2</sub> SrTa <sub>2</sub> O <sub>7</sub> , Li <sub>2</sub> SrNb <sub>2</sub> O <sub>7</sub> ,) Tj E Electrolyte. ChemElectroChem, 2018, 5, 1265-1271.	TQqQQQ 0 r{	gBT <sub>g</sub> /Overlock
143	Highly Conformal Hafnium Silicate Film Growth by Atomic-Layer Chemical Vapor Deposition using a New Combination of Precursors: Hf(OC(CH3)3)4and Si(N(CH3)(C2H5))4. Japanese Journal of Applied Physics, 2006, 45, 5174-5177.	1.5	8
144	n-ZnO:Ga/i-ZnO/p-Si heterojunction light emitting diodes fabricated on patterned Si substrates.	2.2	8

144 Journal of Materials Science: Materials in Electronics, 2009, 20, 1214-1218.

#	Article	IF	CITATIONS
145	Non-destructive micro-Raman analysis of Si near Cu through silicon via. Electronic Materials Letters, 2017, 13, 120-128.	2.2	8
146	Observation of sand movement during bucket installation. International Journal of Physical Modelling in Geotechnics, 2019, 19, 1-14.	0.6	8
147	Controlled Size Growth of Thermally Stable Organometallic Halide Perovskite Microrods: Synergistic Effect of Dual-Doping, Lattice Strain Engineering, Antisolvent Crystallization, and Band Gap Tuning Properties. ACS Omega, 2020, 5, 16106-16119.	3.5	8
148	MOCVD and characterization of Hf-silicate thin films using HTB and TEMAS. Journal of Non-Crystalline Solids, 2007, 353, 1172-1176.	3.1	7
149	Surface Plasmon-Enhanced Light-Emission Mechanism of Ag-Coated ZnO/Al <sub>2</sub> O <sub>3</sub> Core/Shell Nanorod Structures. Journal of Nanoscience and Nanotechnology, 2013, 13, 3335-3340.	0.9	7
150	Improving the electrochemical properties of Al, Zr Co-doped Li4Ti5O12 as a lithium-ion battery anode material. Journal of the Korean Physical Society, 2014, 64, 1545-1549.	0.7	7
151	Passivation analysis of silicon surfaces via sol—gel derived Al-rich ZnO film. Semiconductor Science and Technology, 2015, 30, 015012.	2.0	7
152	Highly Sensitive Micropatterned Interdigitated Electrodes for Enhancing the Concentration Effect Based on Dielectrophoresis. Sensors, 2019, 19, 4152.	3.8	7
153	In-situ growth of nitrogen-doped mesoporous carbon nanostructure supported nickel metal nanoparticles for oxygen evolution reaction in an alkaline electrolyte. Electrochimica Acta, 2019, 306, 617-626.	5.2	7
154	Heterojunction light emitting diodes fabricated with different n-layer oxide structures on p-GaN layers by magnetron sputtering. Applied Surface Science, 2010, 256, 4972-4976.	6.1	6
155	Optical and photovoltaic properties of silicon wire solar cells with controlled ZnO nanorods antireflection coating. Journal of Materials Science, 2012, 47, 4138-4145.	3.7	6
156	Dimensional dependence of phonon transport in freestanding atomic layer systems. Nanoscale, 2013, 5, 11870.	5.6	6
157	Lactamâ€Based HDAC Inhibitors for Anticancer Chemotherapy: Restoration of RUNX3 by Posttranslational Modification and Epigenetic Control. ChemMedChem, 2014, 9, 649-656.	3.2	6
158	A biomemory chip composed of a myoglobin/CNT heterolayer fabricated by the protein-adsorption-precipitation-crosslinking (PAPC) technique. Colloids and Surfaces B: Biointerfaces, 2015, 136, 853-858.	5.0	6
159	Improving luminous efficacy using dual sustain pulse waveform associated with short sustain pulse width in AC-plasma display panels. AIP Advances, 2015, 5, 057119.	1.3	6
160	Significance of N-moieties in regulating the electrochemical properties of nano-porous graphene: Toward highly capacitive energy storage devices. Journal of Industrial and Engineering Chemistry, 2018, 68, 129-139.	5.8	6
161	One-Pot Synthesis of ZnAl Double Hydroxide Powders and Their Calcined Oxide Composites for Lithium-Ion Battery Applications. Science of Advanced Materials, 2017, 9, 1801-1805.	0.7	6
162	Photoelectron spectroscopic analysis of Hf-silicate/SiO[sub 2]â^•Si stacks deposited by atomic layer chemical vapor deposition. Journal of Vacuum Science & Technology B, 2006, 24, 1147.	1.3	5

4

#	Article	IF	CITATIONS
163	Growth and Characterization of Titanium Silicate Nanofilms for Gate Oxide Applications. Journal of Nanoscience and Nanotechnology, 2008, 8, 577-583.	0.9	5
164	Design and Development of ArF Photoresist for Implant Layers. Journal of Photopolymer Science and Technology = [Fotoporima Konwakai Shi], 2010, 23, 259-264.	0.3	5
165	Fabrication of Ordered Silicon Wire Structures via Macropores without Pore Wall by Electrochemical Etching. Journal of the Electrochemical Society, 2011, 159, D37-D45.	2.9	5
166	Fabrication of mesoporous organosilica in a shallow nanotrench for low-k and high elastic modulus material application. Journal of Materials Chemistry, 2012, 22, 21828.	6.7	5
167	Network analysis of photovoltaic-related Science Citation Index papers in Korea. Journal of Renewable and Sustainable Energy, 2015, 7, .	2.0	5
168	Communication—In-Line Detection of Silicon Surface Quality Variation Using Surface Photovoltage and Room Temperature Photoluminescence Measurements. ECS Journal of Solid State Science and Technology, 2016, 5, P438-P440.	1.8	5
169	Comparative Characterization of Crofelemer Samples Using Data Mining and Machine Learning Approaches With Analytical Stability Data Sets. Journal of Pharmaceutical Sciences, 2017, 106, 3270-3279.	3.3	5
170	Highly improved passivation of c-Si surfaces using a gradient <i>i</i> a-Si:H layer. Journal of Applied Physics, 2018, 123, .	2.5	5
171	Effect of atmospheric-pressure plasma treatment on the adhesion properties of a thin adhesive layer in a selective transfer process. Applied Surface Science, 2018, 428, 1141-1148.	6.1	5
172	Evaluation and Optimization of an Image Acquisition System for Dual-Energy Cargo Inspections. IEEE Transactions on Nuclear Science, 2018, 65, 2657-2661.	2.0	5
173	Well-Dispersed ZnFe2O4 Nanoparticles onto Graphene as Superior Anode Materials for Lithium Ion Batteries. Energies, 2019, 12, 304.	3.1	5
174	Structure-based modification of pyrazolone derivatives to inhibit mTORC1 by targeting the leucyl-tRNA synthetase-RagD interaction. Bioorganic Chemistry, 2021, 112, 104907.	4.1	5
175	Optimization Control on Growth Morphology, Lattice Scale Features and Optical Response of Al-Incorporated ZnO Nano-Needles. Nanoscience and Nanotechnology Letters, 2013, 5, 67-72.	0.4	5
176	Electrical and Magnetic Properties of Mn-Doped ZnO. Ferroelectrics, 2002, 273, 71-76.	0.6	4
177	Interfacial properties of ultra thin Zr[sub x]Si[sub 1â^x]O[sub 2] with compositional gradation grown on Si(100) using Zr[N(C[sub 2]H[sub 5])[sub 2]][sub 4] and Si(OC[sub 4]H[sub 9])[sub 4]. Journal of Vacuum Science & Technology an Official Journal of the American Vacuum Society B, Microelectronics Processing and Phenomena, 2004, 22, 2105.	1.6	4
178	Comparison of temporal dark image sticking produced by faceâ€ŧoâ€face and coplanar sustain electrode structures. Journal of Information Display, 2007, 8, 29-33.	4.0	4
179	Optimization of wire array formation in p-type silicon for solar cell application. Current Applied Physics, 2011, 11, S34-S38.	2.4	4
			_

180 Motion estimation with adaptive block size for motion-compensated frame interpolation. , 2012, , .

#	Article	IF	CITATIONS
181	Remarkable increase of thermoelectric power factor using plasma treatment in layered InGaO <sub>3</sub> (ZnO) <i><sub>m</sub></i> thin films. Surface and Interface Analysis, 2012, 44, 1519-1521.	1.8	4
182	Optical properties of hierarchical-nanostructured TiO2 and its time-dependent photo-degradation of gaseous acetaldehyde. Applied Physics Letters, 2013, 103, .	3.3	4
183	Novel Architecture of Plasmon Excitation Based on Self-Assembled Nanoparticle Arrays for Photovoltaics. ACS Applied Materials & Interfaces, 2014, 6, 1030-1035.	8.0	4
184	Intense Ar Plasma Array Jet With Ring-Type Focusing Electrode. IEEE Transactions on Plasma Science, 2014, 42, 2478-2479.	1.3	4
185	Improvement of stability of sinusoidally driven atmospheric pressure plasma jet using auxiliary bias voltage. AIP Advances, 2015, 5, 127141.	1.3	4
186	Discovery of Orally Available Runt-Related Transcription Factor 3 (RUNX3) Modulators for Anticancer Chemotherapy by Epigenetic Activation and Protein Stabilization. Journal of Medicinal Chemistry, 2015, 58, 3512-3521.	6.4	4
187	The administration of high-dose propofol sedation with manual and target-controlled infusion in children undergoing radiation therapy: a 7-year clinical investigation. SpringerPlus, 2016, 5, 376.	1.2	4
188	Improved Comparative Signature Diagrams to Evaluate Similarity of Storage Stability Profiles of Different IgG1 mAbs. Journal of Pharmaceutical Sciences, 2016, 105, 1028-1035.	3.3	4
189	Mid-infrared quantum cascade laser arrays with electrical switching of emission frequencies. AIP Advances, 2018, 8, .	1.3	4
190	Gentianae Macrophyllae Radix Water Extract Inhibits RANKL-Induced Osteoclastogenesis and Osteoclast Specific Genes. Korean Journal of Acupuncture, 2020, 37, 63-75.	0.4	4
191	Growth and Characterization of Hf–Silicate/Al2O3Gate Stacks Grown on Si(100) by Self-Limiting Atomic Layer Deposition. Japanese Journal of Applied Physics, 2006, 45, 7080-7083.	1.5	3
192	Fast intermode decision algorithm based on general and local residual complexity in H.264/AVC. Eurasip Journal on Image and Video Processing, 2013, 2013, .	2.6	3
193	Fabrication and Characterization of Hybrid Si/ZnO Subwavelength Structures as Efficient Antireflection Layer. Journal of Nanoscience and Nanotechnology, 2013, 13, 6359-6361.	0.9	3
194	Dependence of Performance of Si Nanowire Solar Cells on Geometry of the Nanowires. Scientific World Journal, The, 2014, 2014, 1-7.	2.1	3
195	Leakage current behavior in MIM capacitors and MISM organic capacitors with a thin AlOx insulator. Electronic Materials Letters, 2015, 11, 241-245.	2.2	3
196	The Reliability and Degradation of Solar Roadways. , 2018, , .		3
197	Roughness Reduction of PVDF-TrFE Insulator by Reverse Transfer Printing for Enhanced Performance of Ferroelectric Organic Memory Transistors. Journal of Nanoscience and Nanotechnology, 2017, 17, 4149-4152.	0.9	3
198	Impact of solvent on the downconversion efficiency of the N-GQDs/PMMA layer: Application in CIGS solar cells. Optik, 2022, 253, 168569.	2.9	3

#	Article	IF	CITATIONS
199	A comprehensive degradation assessment of silicon photovoltaic modules installed on a concrete base under hot and low-humidity environments: Building applications. Sustainable Energy Technologies and Assessments, 2022, 52, 102314.	2.7	3
200	Conformal growth and characterization of hafnium silicate thin film by MOCVD using HTB (hafnium) Tj ETQq0 0 0 in Electronics, 2007, 18, 391-395.	rgBT /Ov 2.2	erlock 10 Tf 2
201	Enhancing the Performance of Immersion Lithography: Current Challenges and Materials. Journal of Photopolymer Science and Technology = [Fotoporima Konwakai Shi], 2009, 22, 615-617.	0.3	2
202	Refined carbothermal reduction approach for large scale, uniform growth of vertically aligned ZnO nanowires. Physica Status Solidi (A) Applications and Materials Science, 2010, 207, 1854-1858.	1.8	2
203	Dual Surface Discharge Mode for Improving Luminous Efficacy in AC Plasma Display Panel. Japanese Journal of Applied Physics, 2011, 50, 106202.	1.5	2
204	Characteristics of Al-Doped ZnO Films Grown by Atomic Layer Deposition for Silicon Nanowire Photovoltaic Device. Journal of Nanoscience and Nanotechnology, 2012, 12, 5330-5335.	0.9	2
205	Analysis of Weak and Strong Discharge Characteristics for Fast Address Discharge in Microplasma Cells. Molecular Crystals and Liquid Crystals, 2013, 585, 25-33.	0.9	2
206	Evaluation of the density of the charge trapped in organic ferroelectric capacitors based on the Mott-Schottky model. Journal of the Korean Physical Society, 2014, 65, 745-750.	0.7	2
207	Improvement of Current Efficiency at High Field Regime Via Description of Roll-off Characteristic in Model Device of OLEDs. Molecular Crystals and Liquid Crystals, 2014, 599, 79-85.	0.9	2
208	Narrow gap filling in 25 nm shallow trench isolation using highly porous organosilica. Thin Solid Films, 2014, 562, 166-171.	1.8	2
209	Plasma Jet-to-Jet Coupling Behavior Between Two Plasma Jet Arrays for Surface Treatments Requiring Strong Discharge Process. IEEE Transactions on Plasma Science, 2014, 42, 2474-2475.	1.3	2
210	DSP Based Programmable FHD HEVC Decoder. , 2015, , .		2
211	Modification of electrical and piezoelectric properties of ZnO nanorods based on arsenic incorporation via low temperature spin-on-dopant method. Journal of the Korean Physical Society, 2015, 67, 930-935.	0.7	2
212	Direct observation of x-ray radiation-induced damage to SiO2/Si interface using multiwavelength room temperature photoluminescence. Journal of Vacuum Science and Technology B:Nanotechnology and Microelectronics, 2016, 34, 041208.	1.2	2
213	Synthesis of ZnO Nanorods/Carbon Nanofiber Composites Using Electrochemical Deposition for Efficient Supercapacitor Electrodes: Control of Nucleation and Growth of ZnO Nanorods. Journal of Nanoscience and Nanotechnology, 2016, 16, 11669-11673.	0.9	2
214	Solenoid assembly with beam focusing and radiation shielding functions for the 9/6 MeV dual energy linac. Journal of the Korean Physical Society, 2016, 69, 1042-1047.	0.7	2
215	Narrow-linewidth ultra-broadband terahertz sources based on difference-frequency generation in mid-infrared quantum cascade lasers. , 2017, , .		2
216	P-95: Driving Waveform to Reduce Power Consumption in AC-PDP with MgO Single-Crystal Powder. Digest of Technical Papers SID International Symposium, 2010, 41, 1602.	0.3	1

#	Article	IF	CITATIONS
217	PAG Concentration Dependence of the Vertical Density Profile in Photoresist. Journal of Photopolymer Science and Technology = [Fotoporima Konwakai Shi], 2010, 23, 709-713.	0.3	1
218	Fabrication and optimization of Al-doped zinc oxide layer for application in radial p-n junction silicon solar cells. , 2010, , .		1
219	P-96: Analysis of Address Discharge Delay Characteristics Using Transient Characteristics of IR Emission Intensity in Plasma Display Panel. Digest of Technical Papers SID International Symposium, 2011, 42, 1468-1470.	0.3	1
220	Three-Dimensional ICCD Observation of Dual Sustain Discharge Mode in Three-Electrode Microdischarge Cell. IEEE Transactions on Plasma Science, 2011, 39, 2990-2991.	1.3	1
221	Reduction of Power Consumption of Counter Electrode Structure in AC-PDP. Molecular Crystals and Liquid Crystals, 2012, 564, 85-93.	0.9	1
222	An optimal motion vector regularization method using variance-distortion curve. , 2012, , .		1
223	Fabrication of p-Type Silicon Nanowire Arrays with a High Aspect Ratio Using Electrochemical and Alkaline Etching. Journal of Nanoscience and Nanotechnology, 2012, 12, 3567-3570.	0.9	1
224	Improvement of Temporal Image Sticking Characteristics Using Negative Sustain Waveform in AC Plasma Display Panel. IEEE Transactions on Plasma Science, 2012, 40, 1350-1355.	1.3	1
225	Effects of Gas Pressure on Temporal Image Sticking in AC Plasma Display Panel. Molecular Crystals and Liquid Crystals, 2012, 564, 67-75.	0.9	1
226	Morphological Evolution of Silver Nanoparticles and Its Effect on Metal-Induced Chemical Etching of Silicon. Journal of Nanoscience and Nanotechnology, 2013, 13, 3715-3718.	0.9	1
227	Influence of the active layer pattern on the electrical characteristics of organic inverters. Journal of the Korean Physical Society, 2014, 65, 1965-1968.	0.7	1
228	Electrode-Embedded Atmospheric Pressure Plasma Jet Device for Humid Environment. IEEE Transactions on Plasma Science, 2014, 42, 2476-2477.	1.3	1
229	Influence of Gate Dielectric and Its Surface Treatment on Electrical Characteristics of Solution-Processed ZnO Transistors. Journal of Nanoscience and Nanotechnology, 2016, 16, 1848-1851.	0.9	1
230	Influence of overlapped sustain waveform on panel-aging characteristics based on MgO surface morphology variation in alternating-current plasma display panel. Molecular Crystals and Liquid Crystals, 2017, 645, 72-80.	0.9	1
231	Development of seismic CPT for evaluating in-flight soil properties in centrifuge model test. KSCE Journal of Civil Engineering, 2018, 22, 544-554.	1.9	1
232	Fast Simulation Method for Analog Deep Binarized Neural Networks. , 2019, , .		1
233	Universal inherent fluctuations in statistical counting of large particles in slurry used for semiconductor manufacturing. Scientific Reports, 2020, 10, 14731.	3.3	1
234	Electrical and Magnetic Properties of Mn-Doped ZnO. Ferroelectrics, 2002, 273, 71-76.	0.6	1

#	Article	IF	CITATIONS
235	Cu(InGa)Se <sub>2</sub> Photovoltaic Absorber Formation by Spray-Deposition of Aqueous Precursors Followed by Selenization. Journal of Nanoelectronics and Optoelectronics, 2015, 10, 574-577.	0.5	1
236	Difference-Frequency Generation Terahertz Quantum Cascade Lasers with Surface Grating Outcouplers. , 2018, , .		1
237	Impact of Cu Doping on PV Cell Parameters of NiO:Cu Nanostructure-Based Organic-Inorganic Perovskite Solar Cells. , 2020, , .		1
238	Dielectric properties and phase transitions in sr substituted Pb(Mg <sub>1/2</sub> W <sub>1/2</sub> )O <sup>3</sup> . Ferroelectrics, 1999, 223, 179-185.	0.6	0
239	Optical and magnetic properties of laser-deposited semiconducting Zn/sub 1-x/Co/sub x/O thin films. , 0, , .		0
240	GROWTH OF ZIRCONIUM SILICATE THIN FILM BY PULSED-MOCVD USING ZTB AND TDEAS. Surface Review and Letters, 2006, 13, 567-571.	1.1	0
241	Macropore Formation in Prepatterned p-type Silicon. ECS Transactions, 2009, 16, 291-297.	0.5	Ο
242	Minimizing leakage power of sequential circuits through mixed- V t flip-flops and multi- V t combinational gates. ACM Transactions on Design Automation of Electronic Systems, 2009, 15, 1-22.	2.6	0
243	Improvement of Light Extraction Efficiency in n-ZnO:Ga/i-ZnO/p-Si Heterojunction LED Using Truncated Pyramid Patterned Si Substrates. ECS Transactions, 2009, 25, 177-182.	0.5	Ο
244	Macropore Formation in p-type Silicon and Si/SiGe/Si/SiGe/p-type Silicon. ECS Transactions, 2009, 16, 277-283.	0.5	0
245	Vertical Density Profiles of Various Photoresists and Top-coats by X-ray Reflectivity Analysis. Journal of Photopolymer Science and Technology = [Fotoporima Konwakai Shi], 2009, 22, 747-752.	0.3	0
246	P-94: Long Time-Discharge Characteristics of MgO Layer with Nano-Powder in AC Plasma Display Panel. Digest of Technical Papers SID International Symposium, 2010, 41, 1599.	0.3	0
247	Bandwidth-efficient adaptive cache-like buffer architecture in motion compensation for general video codec. , 2011, , .		Ο
248	37.4: Analysis on Address Discharge Characteristics of MgO Layer with MgO Single Crystal Powder under Various Panel Temperatures in AC-PDP. Digest of Technical Papers SID International Symposium, 2011, 42, 510-512.	0.3	0
249	Substrate Effect on the Vertical Density Profile of Thin Photoresist Film. Journal of Photopolymer Science and Technology = [Fotoporima Konwakai Shi], 2011, 24, 159-164.	0.3	Ο
250	Frequency Spectrum Analysis of Corona Discharge Source Measured by Ultrasound Detector. Communications in Computer and Information Science, 2012, , 294-299.	0.5	0
251	Investigation of Address Discharge and Efficiency Characteristics by Thickness of Phosphor Layer in Microplasma Cells. Molecular Crystals and Liquid Crystals, 2012, 564, 104-111.	0.9	0
252	Short pulse type dual sustain discharge waveform for improving discharge efficiency in		0

microdischarge cell. , 2012, , .

#	Article	IF	CITATIONS
253	Temporal Bright and Dark Image Sticking Phenomena of Counter-type Electrodes with Parallel Electric Field in AC-PDP. Molecular Crystals and Liquid Crystals, 2012, 564, 94-103.	0.9	0
254	Influence of Surface Contamination on the Electrical Breakdown between Ag Electrodes in AC Plasma Display Panels. Molecular Crystals and Liquid Crystals, 2013, 585, 34-40.	0.9	0
255	Effects of Operating Frequency on Panel-Aging and Discharge Characteristics in AC Plasma Display Panel. Molecular Crystals and Liquid Crystals, 2013, 585, 41-49.	0.9	0
256	Solvent-Tolerant Patterning of Poly(3-hexylthiophene) Film by Subtractive Photolithography. Molecular Crystals and Liquid Crystals, 2014, 599, 36-42.	0.9	0
257	Monolithically patterned high mobility solution-processed metal-oxide TFTs with metallic capping layers. , 2014, , .		0
258	Cost-Effective Local Dimming Driving Scheme of Xe-Lamp for Low-Power Backlight Unit. Molecular Crystals and Liquid Crystals, 2015, 617, 147-157.	0.9	0
259	Address Discharge Characteristics by Changes in Sustain Pulse Numbers in Plasma Display Panel with High Xe Contents. Molecular Crystals and Liquid Crystals, 2015, 617, 158-167.	0.9	0
260	Influences of MgO Thicknesses Variation on Degradation Characteristics during Long-term Discharge in Microdischarge Cells. Molecular Crystals and Liquid Crystals, 2015, 617, 109-118.	0.9	0
261	Modified Driving Waveform for Stable High-Speed Address Discharge in AC PDP under High Xe Gas Mixture. Molecular Crystals and Liquid Crystals, 2015, 617, 119-129.	0.9	0
262	Ultra-low-power voice trigger for wearable devices. , 2015, , .		0
263	Spectroscopic study of terahertz difference-frequency nonlinear susceptibility in mid-infrared quantum cascade lasers. , 2016, , .		0
264	Terahertz difference frequency generation in quantum cascade lasers on silicon. , 2017, , .		0
265	Analysis on electron emission characteristics of MgO layer with MgO crystal powder under various panel temperatures in ac-plasma display panels. Molecular Crystals and Liquid Crystals, 2017, 645, 102-111.	0.9	0
266	Improvement in Surface Passivation of c-Si Using Gradient-Layered a-Si:H Film for High Efficiency Silicon Heterojunction Solar Cells. , 2017, , .		0
267	Effects of MgO Nanocrystal Powder on Long-Term Sustain and Address Discharge Characteristics in ac-Plasma Display Panel. Journal of Nanoscience and Nanotechnology, 2017, 17, 335-340.	0.9	0
268	Selfie Stitch: Dual Homography Based Image Stitching for Wide-Angle Selfie. , 2018, , .		0
269	Pâ€136: Resistive Type 2D Mapping Positional Strain Sensor Array for Advanced Tactile Displays. Digest of Technical Papers SID International Symposium, 2018, 49, 1909-1912.	0.3	0
270	An RRAM-based Analog Neuron Design for the Weighted Spiking Neural network. , 2019, , .		0

#	Article	IF	CITATIONS
271	A STUDY OF GUIDED ULTRASONIC WAVE APPLICATION FOR HEAT EXCHANGER PERFORMANCE IMPROVEMENT. , 2008, , .		0
272	Difference-Frequency Generation Quantum Cascade Laser Sources on Silicon. , 2017, , .		0
273	1.9 THz Difference-Frequency Generation in Mid-Infrared Quantum Cascade Lasers with Grating Outcouplers. , 2017, , .		0
274	Mid-infrared quantum cascade lasers transfer-printed on silicon-on-sapphire. , 2017, , .		0
275	Efficient THz Generation in Long-Wavelength Infrared Quantum Cascade Lasers. , 2017, , .		0
276	Broadly tunable terahertz difference-frequency generation in quantum cascade lasers on silicon. Optical Engineering, 2017, 57, 1.	1.0	0